Electr Eng
DOI 10.1007/s00202-017-0511-9

ORIGINAL PAPER

Sensorless speed control of five-phase PMSM drives with low current distortion

Kamel Saleh[1] · **Mark Sumner**[2]

Received: 18 August 2016 / Accepted: 2 February 2017

Abstract This paper introduces a design of a sensorless control of a five-phase permanent magnet synchronous motor drive working at low and zero speeds with low current distortion. The rotor position is obtained through tracking the saturation saliency. The saliency position is tracked through measuring the dynamic current response of the motor line currents due to the insulated-gate bipolar transistor switching actions. It uses the fundamental pulse width modulation (PWM) waveform obtained using the multi-phase space vector pulse width modulation only. The saliency tracking algorithm used in this paper does not only improve the quality of the estimated position signals but also guarantees a minimum current distortion. It reduces the modifications introduced on the PWM waveform. Simulation results are provided to verify the effectiveness of the proposed design over a wide speed range under different load conditions.

Keywords Sensorless · Five-phase motor · Multi-dimension SVPWM · THD

1 Introduction

The interest in multi-phase motor drives has increased in recent years. These motors offer several advantages when compared to three-phase machines such as improving reliability, efficiency, torque density, and reducing torque pulsations [1,2]. Therefore, multi-phase motor drives are extensively considered for applications related to vehicles, aerospace application (more electric craft), ship propulsion, and high-power applications. The modulation technique that is proposed to be used in multi-phase motor drives is multi-dimension SVPWM. This modulation technique is based on the concept of orthogonal multi-dimensional vector space [3–12] in which the voltage vectors are synthesized both in d–q subspace and in other subspace. Many control techniques have been adopted to control the multi-phase motor drives in a sensored mode such as fuzzy logic control [13] and predictive current control [14].

In the last couple of years, few researchers have been directed toward the sensorless control of multi-phase electrical drives. These researches focus on the model-based sensorless control, direct torque control, and high-frequency injections[15–19].

This paper introduces a new method to track the saturation saliency in five-phase PMSM drives. The saliency position is obtained through measuring the dynamic current responses of the motor due to the IGBTs switching actions [20–22]. It uses the fundamental PWM waveform obtained using the multi-phase space vector pulse width modulation only. The saliency tracking algorithm used in the proposed method does not only improve the quality of the estimated position signals but also guarantees a minimum current distortion in the motor currents. It reduces the modifications introduced on the PWM waveform.

2 Research method

2.1 Five-phase converter drive topology

Figure 1 shows the proposed five-phase converter drive topology [21]. The motor model is given by (1)–(30).

✉ Kamel Saleh
kamel.saleh@najah.edu

[1] Electrical Engineering Department, An-Najah National University, Nablus, West Bank, Palestine

[2] Electrical Engineering Department, Nottingham University, Nottingham, UK

Published online: 14 February 2017

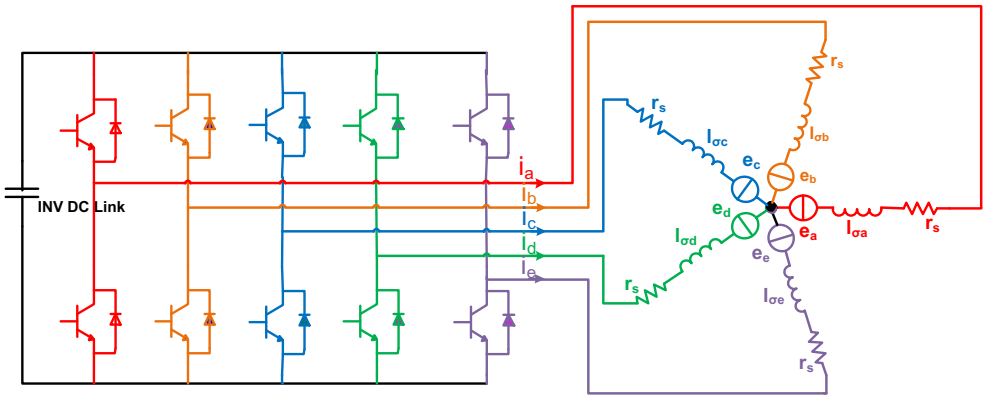

Fig. 1 Five-phase converter drive topology

$$v_a = r_s \times i_a + \frac{d\varphi_a}{dt}, \tag{1}$$

$$v_b = r_s \times i_b + \frac{d\varphi_b}{dt}, \tag{2}$$

$$v_c = r_s \times i_c + \frac{d\varphi_c}{dt} \tag{3}$$

$$v_d = r_s \times i_d + \frac{d\varphi_d}{dt}, \tag{4}$$

$$v_e = r_s \times i_e + \frac{d\varphi_e}{dt} \tag{5}$$

where v_a, v_b, v_c, v_d, v_e are the external voltages applied to the motor, r_s is the equivalent resistance of the stator phase winding, i_a, i_b, i_c, i_d, i_e are the stator phase currents, $\frac{d\varphi_a}{dt}, \frac{d\varphi_b}{dt}, \frac{d\varphi_c}{dt}, \frac{d\varphi_d}{dt}, \frac{d\varphi_e}{dt}$ are the rate of changes in the magnetic flux in the phases. The permanent magnet and the five windings contribute to the total flux linking each winding as given:

$$\varphi_a = L_{aa} \times i_a + L_{ab} \times i_b + L_{ac} \times i_c + L_{ad} \times i_d + L_{ae} \times i_e + \varphi_{ma} \tag{6}$$

$$\varphi_b = L_{ab} \times i_a + L_{bb} \times i_b + L_{bc} \times i_c + L_{bd} \times i_d + L_{be} \times i_e + \varphi_{mb} \tag{7}$$

$$\varphi_c = L_{ac} \times i_a + L_{bc} \times i_b + L_{cc} \times i_c + L_{cd} \times i_d + L_{ce} \times i_e + \varphi_{mc} \tag{8}$$

$$\varphi_d = L_{ad} \times i_a + L_{bd} \times i_b + L_{cd} \times i_c + L_{dd} \times i_d + L_{de} \times i_e + \varphi_{md} \tag{9}$$

$$\varphi_e = L_{ae} \times i_a + L_{be} \times i_b + L_{ce} \times i_c + L_{de} \times i_d + L_{ee} \times i_e + \varphi_{me} \tag{10}$$

where $\varphi_a, \varphi_b, \varphi_c, \varphi_d$, and φ_e are the total fluxes linking each stator windings.

L_{aa}, L_{bb}, L_{cc}, L_{dd}, and L_{ee} are the self-inductances of the stator windings.

L_{ab}, L_{ac}, L_{ba}, L_{ad}, L_{ae}, L_{bc}, L_{bd}, L_{be}, L_{cd}, L_{ce} and L_{de} are the mutual inductances of the stator windings. $\varphi_{ma}, \varphi_{mb}, \varphi_{mc}, \varphi_{md}$, and φ_{me} are the permanent magnet fluxes linking the stator windings.

The inductances in the stator windings are functions of rotor angle, defined by

$$L_{aa} = L_{so} + L_{sl} + L_x \cos(2\theta), \tag{11}$$

$$L_{bb} = L_{so} + L_{sl} + L_x \cos\left(2\theta - 72^\circ\right) \tag{12}$$

$$L_{cc} = L_{so} + L_{sl} + L_x \cos\left(2\theta - 144^\circ\right), \tag{13}$$

$$L_{dd} = L_{so} + L_{sl} + L_x \cos\left(2\theta - 216^\circ\right) \tag{14}$$

$$L_{ee} = L_{so} + L_{sl} + L_x \cos\left(2\theta - 288^\circ\right), \tag{15}$$

$$L_{ab} = L_{so} \cos(72^\circ) + L_x \cos\left(2\theta - 72^\circ\right) \tag{16}$$

$$L_{ac} = L_{so} \cos(144^\circ) + L_x \cos\left(2\theta - 144^\circ\right), \tag{17}$$

$$L_{ad} = L_{so} \cos(216^\circ) + L_x \cos\left(2\theta - 216^\circ\right) \tag{18}$$

$$L_{ae} = L_{so} \cos(288^\circ) + L_x \cos\left(2\theta + 288^\circ\right), \tag{19}$$

$$L_{bc} = L_{so} \cos(72^\circ) + L_x \cos\left(2\theta - 216^\circ\right) \tag{20}$$

$$L_{bd} = L_{so} \cos(144^\circ) + L_x \cos\left(2\theta - 288^\circ\right), \tag{21}$$

$$L_{be} = L_{so} \cos(144^\circ) + L_x \cos(2\theta) \tag{22}$$

$$L_{cd} = L_{so} \cos(72^\circ) + L_x \cos(2\theta), \tag{23}$$

$$L_{ce} = L_{so} \cos(144^\circ) + L_x \cos\left(2\theta - 72^\circ\right) \tag{24}$$

$$L_{de} = L_{so} \cos(72^\circ) + L_x \cos(2\theta - 144) \tag{25}$$

where L_{sl} is the stator self-inductance per phase. This is the average self-inductance of each of the stator windings. L_x is the stator inductance fluctuation. L_{so} is the stator mutual inductance. This is the average mutual inductance between the stator windings. The effects of saturation saliency appeared in stator self and mutual inductances are indicated by the term (2θ).

The flux linkages at the stator windings due to the permanent magnet are

$$\varphi_{ma} = \Lambda_m \times \cos(\theta), \tag{26}$$

$$\varphi_{mb} = \Lambda_m \times \cos\left(\theta - 72^{\circ}\right), \tag{27}$$

$$\varphi_{mc} = \Lambda_m \times \cos\left(\theta - 144^{\circ}\right). \tag{28}$$

$$\varphi_{md} = \Lambda_m \times \cos(\theta - 216), \tag{29}$$

$$\varphi_{me} = \Lambda_m \times \cos\left(\theta - 288^{\circ}\right). \tag{30}$$

where φ_m is the peak flux linkage due to permanent magnet.

2.2 Multi-phase space vector pulse width modulation

2.2.1 Concept of orthogonal vector space

The kth order harmonics ($k = 5 \times m \pm 2, m = 1, 3, 5\ldots$) of the machine's variables such as phase voltage and phase current do not produce any rotating MMF (not electromechanical energy conversion-related). These harmonics will freely flow through the windings of the five-phase motor. Their amplitudes will be restricted by the stator leakage impedance only [3–12,15–19]. Hence, generation of certain low-order voltage harmonics (third harmonic) in the voltage source inverter (VSI) output can lead to large third harmonic in stator current. It is, therefore, important that the multiphase VSI output is kept as close as possible to sinusoidal. To do so, the reference voltage should be mapped into two orthogonal planes. The first one is the $d1$–$q1$ plane. This plane is rotating at synchronous speed and has fundamental components of the reference voltage. The second is the $d3$–$q3$ plane. It is rotating at a speed equals to 3 times the synchronous speed and has the third harmonic components of the reference voltage using the transformation given in (31) and (32):

$$\begin{bmatrix} d1 \\ q1 \\ d3 \\ q3 \end{bmatrix} = [G] \begin{bmatrix} a \\ b \\ c \\ d \\ e \end{bmatrix} \tag{31}$$

and

$$\begin{bmatrix} a \\ b \\ c \\ d \\ e \end{bmatrix} = \left[G^{-1}\right] \begin{bmatrix} d1 \\ q1 \\ d3 \\ q3 \end{bmatrix} \tag{32}$$

where

$$\mathrm{G} = \frac{2}{5} \begin{bmatrix} \sin(\theta) & \sin(\theta - 72^{\circ}) & \sin(\theta - 144^{\circ}) & \sin(\theta - 216^{\circ}) & \sin(\theta - 288^{\circ}) \\ \cos(\theta) & \cos(\theta - 72^{\circ}) & \cos(\theta - 144^{\circ}) & \cos(\theta - 216^{\circ}) & \cos(\theta - 288^{\circ}) \\ \sin(3\theta) & \sin(3(\theta - 72^{\circ})) & \sin(3(\theta - 144^{\circ})) & \sin(3(\theta - 216^{\circ})) & \sin(3((\theta - 288^{\circ})) \\ \cos(3\theta) & \cos(3(\theta - 72^{\circ})) & \cos(3(\theta - 144^{\circ})) & \cos(3(\theta - 216^{\circ})) & \cos(3(\theta - 288^{\circ})) \end{bmatrix} \tag{33}$$

As the two planes $d1$–$q1$ and $d3$–$q3$ are orthogonal, the fundamental and the third harmonic components of the voltage can be controlled independently. Also, the reference voltage can be mapped into two orthogonal stationary frames $\alpha1$–$\beta1$ and $\alpha3$–$\beta1$ according to (34–36).

$$\begin{bmatrix} \alpha1 \\ \beta1 \\ \alpha3 \\ \beta3 \end{bmatrix} = [H] \begin{bmatrix} a \\ b \\ c \\ d \\ e \end{bmatrix} \tag{34}$$

and

$$\begin{bmatrix} a \\ b \\ c \\ d \\ e \end{bmatrix} = \left[H^{-1}\right] \begin{bmatrix} \alpha1 \\ \beta1 \\ \alpha3 \\ \beta3 \end{bmatrix}, \tag{35}$$

where

$$H = \frac{2}{5} \begin{bmatrix} 1 & \cos(72^{\circ}) & \cos(144^{\circ}) & \cos(216^{\circ}) & \cos(288^{\circ}) \\ 0 & \sin(72^{\circ}) & \sin(144^{\circ}) & \sin(216^{\circ}) & \sin(288^{\circ}) \\ 1 & \cos(216^{\circ}) & \cos(72^{\circ}) & \cos(288^{\circ}) & \cos(144^{\circ}) \\ 0 & \sin(216^{\circ}) & \sin(72^{\circ}) & \sin(288^{\circ}) & \sin(144^{\circ}) \end{bmatrix} \tag{36}$$

As noted in Eqs (34–36), there are 32 space vectors two of which are zero vectors (00000 and 11111). The other 30 nonzero space voltage vectors can be projected to $\alpha1$–$\beta1$ plane and $\alpha3$–$\beta1$ plane as shown in Fig. 2. In $\alpha1$–$\beta1$ plane, the 30 vectors are composed of three sets of different amplitude vectors. These vectors divide $\alpha1$–$\beta1$ plane into 10 sectors. The amplitudes of these voltage vectors are [3–12,15]:

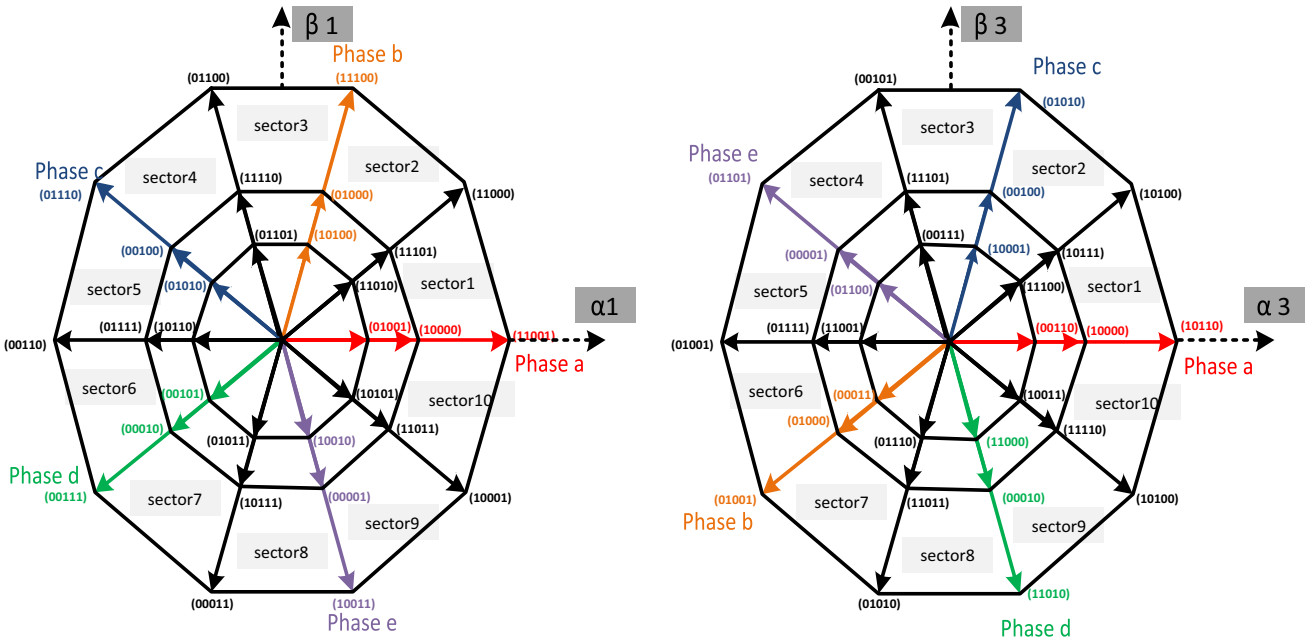

Fig. 2 Thirty nonzero switching vectors on $\alpha 1$–$\beta 1$ plane and $\alpha 3$–$\beta 3$ plane

$V_{\min} = 0.2472V_{\mathrm{dc}}$, (11001), (11000), (11100), (01100), (01110), (00110), (00111), (00011), (10011), (10001).

$V_{\mathrm{mid}} = 0.4V_{\mathrm{dc}}$, (10000), (11101), (01000), (11110), (00100), (01111), (00010), (10111), (00001), (11011).

$V_{\max} = 0.6472V_{\mathrm{dc}}$, (01001), (11010), (10100), (01101), (01010), (10110), (00101), (01011), (10010), (10101).

And the ratio of the amplitudes is 1:1.618:1.6182. It is the same situation in the $\alpha 3$–$\beta 1$ plane.

From the average vector concept during one sampling period [12], a reference voltage vector in the $\alpha 1$–$\beta 1$ plane can be realized by adjusting the application times of the nearest two V_{mid} switching vectors and two $V_{\max}$ switching vectors. The other combinations of switching vectors increase the number of switching or decrease the maximum magnitude of the realizable voltage vector.

2.2.2 *Calculation of the application times for the switching vectors*

Figure 3 shows the reference voltage of the fundamental component ($V_{\mathrm{ref}}\_\alpha 1$–$\beta 1$) that exists in the first sector in the $\alpha 1$–$\beta 1$ plane and the third harmonic component of the reference voltage ($V_{\mathrm{ref}}\_\alpha 3$–$\beta 3$) located in the first sector in the $\alpha 3$–$\beta 1$ plane. For both reference voltages, the vectors (00000, 10000, 11000, 01001, 11101, 11111) are used to utilize them in both $\alpha 1$–$\beta 1$ and $\alpha 3$–$\beta 3$ planes as shown in Fig. 3.

The time needed for applying each vector can be calculated as:

$$\begin{bmatrix} T_1 \\ T_2 \\ T_3 \\ T_4 \end{bmatrix} = T_s \times \left[T^{-1}\right] \begin{bmatrix} V_{\mathrm{ref}}\_\alpha 1 \\ V_{\mathrm{ref}}\_\beta 1 \\ V_{\mathrm{ref}}\_\alpha 3 \\ V_{\mathrm{ref}}\_\beta 3 \end{bmatrix} \tag{37}$$

where

$$\mathrm{T} = \begin{bmatrix} V_{\mathrm{mid}} & V_{\max}\cos(72^\circ) & V_{\max} & V_{\mathrm{mid}}\cos(72^\circ) \\ 0 & V_{\max}\sin(72^\circ) & 0 & V_{\mathrm{mid}}\sin(72^\circ) \\ V_{\mathrm{mid}} & V_{\min}\cos(288^\circ) & -V_{\min} & V_{\mathrm{mid}}\cos(108^\circ) \\ 0 & V_{\min}\sin(288^\circ) & 0 & V_{\mathrm{mid}}\sin(108^\circ) \end{bmatrix} \tag{38}$$

$$T_0 = T_s - T_1 - T_2 - T_3 - T_4. \tag{39}$$

The same approach can be applied for other sectors.

2.3 Algorithm for tracking the saturation saliency of five-phase PMSM

The stator windings self-inductances are modulated by the anisotropy obtained by the saturation saliency of main flux as shown in (11–15). This modulation will be reflected in the transient response of the motor line currents due to the test vector imposed by the inverter. So by measuring the transient current response to the active vectors, it is possible to detect the inductance variation and track the rotor position. It is worth saying that the output PWM waveform obtained using the multi-dimension SVPWM in this work has four active vectors $V1$, $V2$, $V3$, and $V4$ in addition to the zero vector $V0$. This number of active vectors makes it possible to obtain more than one algorithm to track the saturation saliency. This paper introduces the following algorithms:

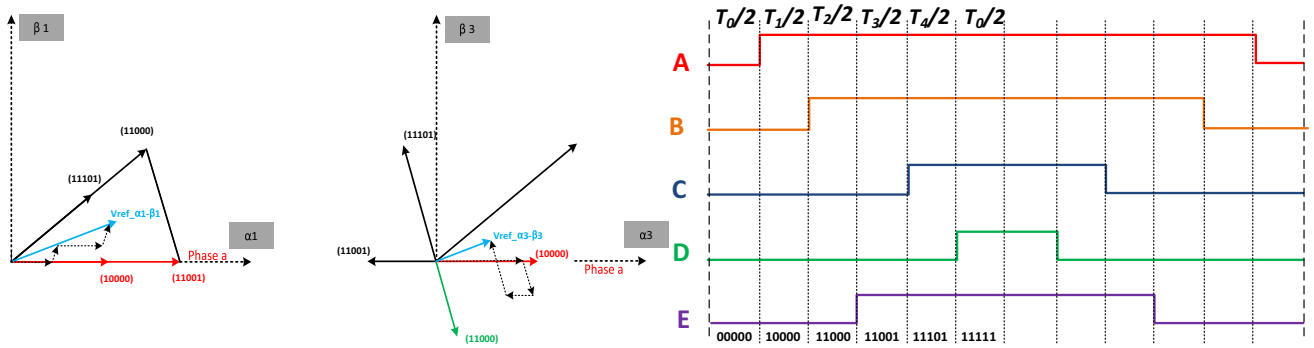

Fig. 3 Realization of a reference voltage vector located in sector 1 on the *d*–*q* plane and the associated switching sequence

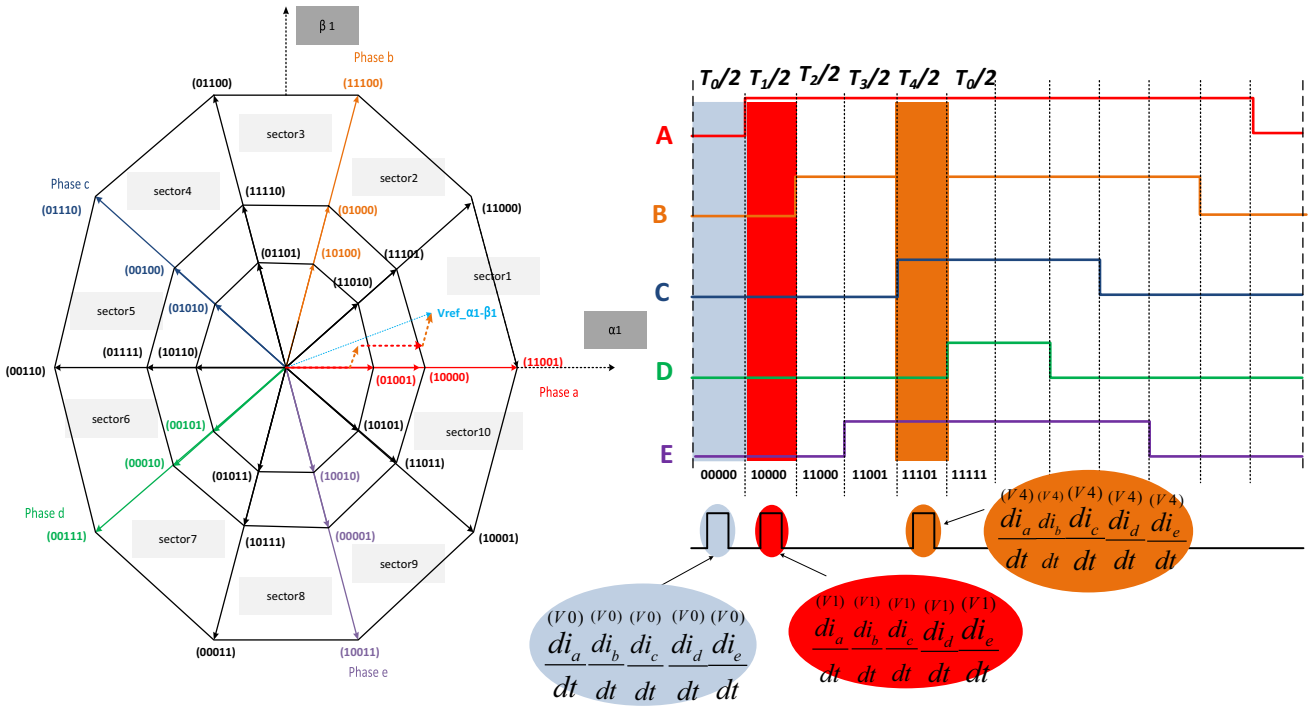

Fig. 4 Sampling time of the currents responses due to the switching actions of active vector $V1$ and $V4$ in case that V_ref_α1-β1 exists in first sector

2.3.1 Tracking saliency using the active vectors V1, V4 and V0

Figure 4 shows the space vector modulation state diagram for a five-phase inverter when V_ref_α1-β1 exists in the first sector. The switching sequences and the timing of the applied vectors are shown in Fig. 4.

Figure 5a–c shows, respectively, the stator circuits when the vectors $V0$, $V1$, and $V4$ are applied.

Using the circuit in Fig. 5a, the following equations hold true:

$$0 = r_s * i_a^{(V0)} + l_{\sigma a} * \frac{\mathrm{d}i_a^{(V0)}}{\mathrm{d}t} + e_a^{(V0)} - r_s * i_b^{(V0)} - l_{\sigma b} * \frac{\mathrm{d}i_b^{(V0)}}{\mathrm{d}t} - e_b^{(V0)} \tag{40}$$

$$0 = r_s * i_b^{(V0)} + l_{\sigma b} * \frac{\mathrm{d}i_b^{(V0)}}{\mathrm{d}t} + e_b^{(V0)} - r_s * i_c^{(V0)} - l_{\sigma c} * \frac{\mathrm{d}i_c^{(V0)}}{\mathrm{d}t} - e_c^{(V0)} \tag{41}$$

$$0 = r_s * i_c^{(V0)} + l_{\sigma c} * \frac{\mathrm{d}i_c^{(V0)}}{\mathrm{d}t} + e_c^{(V0)} - r_s * i_d^{(V0)} - l_{\sigma d} * \frac{\mathrm{d}i_d^{(V0)}}{\mathrm{d}t} - e_d^{(V0)} \tag{42}$$

$$0 = r_s * i_d^{(V0)} + l_{\sigma d} * \frac{\mathrm{d}i_d^{(V0)}}{\mathrm{d}t} + e_d^{(V0)} - r_s * i_e^{(V0)} - l_{\sigma e} * \frac{\mathrm{d}i_e^{(V0)}}{\mathrm{d}t} - e_e^{(V0)} \tag{43}$$

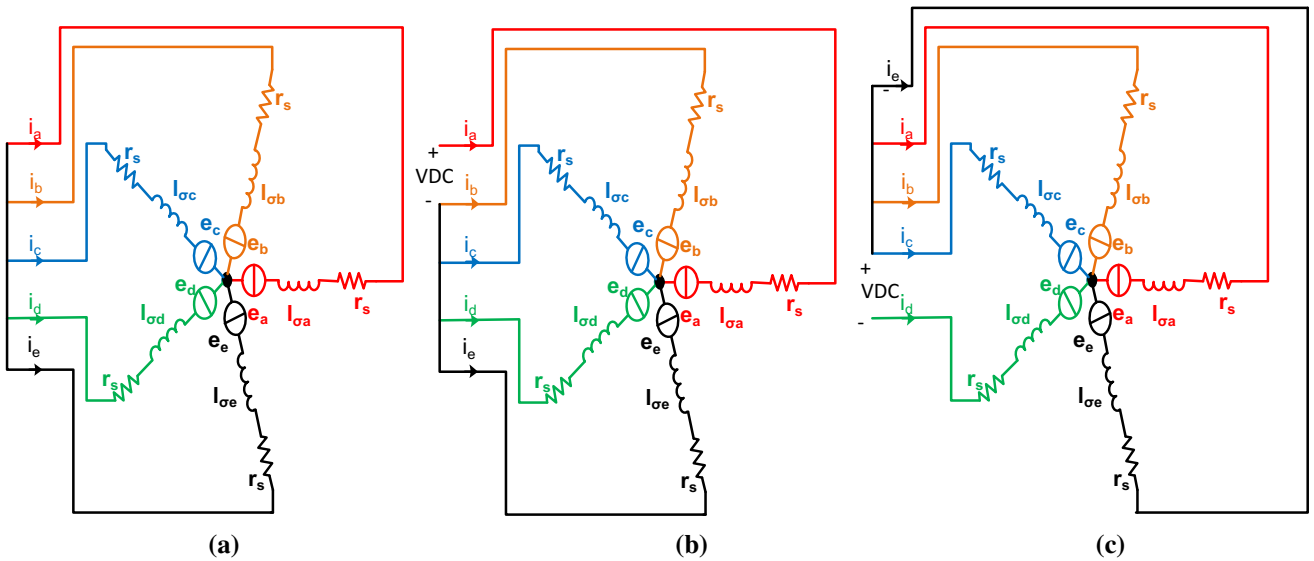

Fig. 5 Stator circuits when: **a** $V0$ is applied; **b** $V1$ is applied; **c** $V4$ is applied

$$0 = r_s * i_e^{(V0)} + l_{\sigma e} * \frac{di_e^{(V0)}}{dt} + e_e^{(V0)} - r_s * i_a^{(V0)} - l_{\sigma a} * \frac{di_a^{(V0)}}{dt} - e_a^{(V0)} \tag{44}$$

The following equations are obtained using Fig. 5b:

$$V_{DC} = r_s * i_a^{(V1)} + l_{\sigma a} * \frac{di_a^{(V1)}}{dt} + e_a^{(V1)} - r_s * i_b^{(V1)} - l_{\sigma b} * \frac{di_b^{(V1)}}{dt} - e_b^{(V1)} \tag{45}$$

$$0 = r_s * i_b^{(V1)} + l_{\sigma b} * \frac{di_b^{(V1)}}{dt} + e_b^{(V1)} - r_s * i_c^{(V1)} - l_{\sigma c} * \frac{di_c^{(V1)}}{dt} - e_c^{(V1)} \tag{46}$$

$$0 = r_s * i_c^{(V1)} + l_{\sigma c} * \frac{di_c^{(V1)}}{dt} + e_c^{(V1)} - r_s * i_d^{(V1)} - l_{\sigma d} * \frac{di_d^{(V1)}}{dt} - e_d^{(V1)} \tag{47}$$

$$0 = r_s * i_d^{(V1)} + l_{\sigma d} * \frac{di_d^{(V1)}}{dt} + e_d^{(V1)} - r_s * i_e^{(V1)} + l_{\sigma e} * \frac{di_e^{(V1)}}{dt} - e_e^{(V1)} \tag{48}$$

$$-V_{DC} = r_s * i_e^{(V1)} + l_{\sigma e} * \frac{di_e^{(V1)}}{dt} + e_e^{(V1)} - r_s * i_a^{(V1)} - l_{\sigma a} * \frac{di_a^{(V1)}}{dt} - e_a^{(V1)} \tag{49}$$

Finally, when $V4$ is applied as shown in Fig. 5c, the following equations hold true:

$$0 = r_s * i_a^{(V4)} + l_{\sigma a} * \frac{di_a^{(V4)}}{dt} + e_a^{(V4)} - r_s * i_b^{(V4)} - l_{\sigma b} * \frac{di_b^{(V4)}}{dt} - e_b^{(V4)} \tag{50}$$

$$0 = r_s * i_b^{(V4)} + l_{\sigma b} * \frac{di_b^{(V4)}}{dt} + e_b^{(V4)} - r_s * i_c^{(V4)} - l_{\sigma c} * \frac{di_c^{(V4)}}{dt} - e_c^{(V4)} \tag{51}$$

$$V_{DC} = r_s * i_c^{(V4)} + l_{\sigma c} * \frac{di_c^{(V4)}}{dt} + e_c^{(V4)} - r_s * i_d^{(V4)} - l_{\sigma d} * \frac{di_d^{(V4)}}{dt} - e_d^{(V4)} \tag{52}$$

$$-V_{DC} = r_s * i_d^{(V4)} + l_{\sigma d} * \frac{di_d^{(V4)}}{dt} + e_d^{(V4)} - r_s * i_e^{(V4)} - l_{\sigma e} * \frac{di_e^{(V4)}}{dt} - e_e^{(V4)} \tag{53}$$

$$0 = r_s * i_e^{(V4)} + l_{\sigma e} * \frac{di_e^{(V4)}}{dt} + e_e^{(V4)} - r_s * i_a^{(V4)} - l_{\sigma a} * \frac{di_a^{(V4)}}{dt} - e_a^{(V4)} \tag{54}$$

Assuming that the voltage drop across the stator resistances is small and the back emf can be neglected providing the time separation between the vectors is small, the following equations can be obtained using vector $V1$, $V4$ and $V0$:

$$P_a = -\left(\frac{di_c^{(V4)}}{dt} - \frac{di_c^{(V0)}}{dt}\right) = C1 + C2 * \cos(2\theta) \tag{55}$$

$$P_b = -\left(\frac{di_e^{(V4)}}{dt} - \frac{di_e^{(V0)}}{dt}\right) = C1 + C2 * \cos\left(2\theta - 72^\circ\right) \tag{56}$$

$$P_c = \left(\frac{\mathrm{d}i_e^{(V1)}}{\mathrm{d}t} - \frac{\mathrm{d}i_e^{(V0)}}{\mathrm{d}t}\right) = C1 + C2 * \cos\left(2\theta - 144^\circ\right) \quad (57)$$

$$P_d = \left(\frac{\mathrm{d}i_b^{(V1)}}{\mathrm{d}t} - \frac{\mathrm{d}i_b^{(V0)}}{\mathrm{d}t}\right) = C1 + C2 * \cos\left(2\theta - 216^\circ\right) \quad (58)$$

where:

$$C1 = \frac{-\mathrm{V}_{DC} * (L_{so} + L_{sl})^3}{5\left((L_{so} + L_{sl})^4 + \frac{3}{4} * (L_{so} + L_{sl})^2 * L_x^2 + 0.0506\right)} \quad (59)$$

$$C2 = \frac{-\mathrm{V}_{DC} * 1.618 * (L_{so} + L_{sl})^2 * L_x}{5\left((L_{so} + L_{sl})^4 + \frac{3}{4} * (L_{so} + L_{sl})^2 * L_x^2 + 0.0506\right)} \quad (60)$$

The estimated position signal P_a, P_b, P_c, P_d, and P_e in other sectors can be obtained using the same technique as shown in Table 1.

2.3.2 Tracking saliency using the vectors V2, V3, and V0

Figure 6 shows the space vector modulation state diagram for a five-phase inverter when V_ref_α1-β1 exists in the first sector. The switching sequences and the timing of the applied vectors will be :

The stator circuits when the vectors $V0$, $V2$, and $V3$ are applied are shown in Fig. 7a–c, respectively.

Using the circuit in Fig. 7a, the following equations hold true:

$$0 = r_s * i_a^{(V0)} + l_{\sigma a} * \frac{\mathrm{d}i_a^{(V0)}}{\mathrm{d}t} + e_a^{(V0)} - r_s * i_b^{(V0)} - l_{\sigma b} * \frac{\mathrm{d}i_b^{(V0)}}{\mathrm{d}t} - e_b^{(V0)} \quad (61)$$

$$0 = r_s * i_b^{(V0)} + l_{\sigma b} * \frac{\mathrm{d}i_b^{(V0)}}{\mathrm{d}t} + e_b^{(V0)} - r_s * i_c^{(V0)} - l_{\sigma c} * \frac{\mathrm{d}i_c^{(V0)}}{\mathrm{d}t} - e_c^{(V0)} \quad (62)$$

$$0 = r_s * i_c^{(V0)} + l_{\sigma c} * \frac{\mathrm{d}i_c^{(V0)}}{\mathrm{d}t} + e_c^{(V0)} - r_s * i_d^{(V0)} - l_{\sigma d} * \frac{\mathrm{d}i_d^{(V0)}}{\mathrm{d}t} - e_d^{(V0)} \quad (63)$$

$$0 = r_s * i_d^{(V0)} + l_{\sigma d} * \frac{\mathrm{d}i_d^{(V0)}}{\mathrm{d}t} + e_d^{(V0)} - r_s * i_e^{(V0)} - l_{\sigma e} * \frac{\mathrm{d}i_e^{(V0)}}{\mathrm{d}t} - e_e^{(V0)} \quad (64)$$

$$0 = r_s * i_e^{(V0)} + l_{\sigma e} * \frac{\mathrm{d}i_e^{(V0)}}{\mathrm{d}t} + e_e^{(V0)} - r_s * i_a^{(V0)} - l_{\sigma a} * \frac{\mathrm{d}i_a^{(V0)}}{\mathrm{d}t} - e_a^{(V0)} \quad (65)$$

The following equations are obtained using Fig. 7b:

$$0 = r_s * i_a^{(V2)} + l_{\sigma a} * \frac{\mathrm{d}i_a^{(V2)}}{\mathrm{d}t} + e_a^{(V1)} - r_s * i_b^{(V2)} - l_{\sigma b} * \frac{\mathrm{d}i_b^{(V2)}}{\mathrm{d}t} - e_b^{(V2)} \quad (66)$$

$$\mathrm{V}_{DC} = r_s * i_b^{(V2)} + l_{\sigma b} * \frac{\mathrm{d}i_b^{(V2)}}{\mathrm{d}t} + e_b^{(V2)} - r_s * i_c^{(V2)} - l_{\sigma c} * \frac{\mathrm{d}i_c^{(V2)}}{\mathrm{d}t} - e_c^{(V2)} \quad (67)$$

$$0 = r_s * i_c^{(V2)} + l_{\sigma c} * \frac{\mathrm{d}i_c^{(V2)}}{\mathrm{d}t} + e_c^{(V2)} - r_s * i_d^{(V2)} - l_{\sigma d} * \frac{\mathrm{d}i_d^{(V2)}}{\mathrm{d}t} - e_d^{(V2)} \quad (68)$$

$$0 = r_s * i_d^{(V2)} + l_{\sigma d} * \frac{\mathrm{d}i_d^{(V2)}}{\mathrm{d}t} + e_d^{(V2)} - r_s * i_e^{(V2)} + l_{\sigma e} * \frac{\mathrm{d}i_e^{(V2)}}{\mathrm{d}t} - e_e^{(V2)} \quad (69)$$

$$-\mathrm{V}_{DC} = r_s * i_e^{(V2)} + l_{\sigma e} * \frac{\mathrm{d}i_e^{(V2)}}{\mathrm{d}t} + e_e^{(V2)} - r_s * i_a^{(V2)} - l_{\sigma a} * \frac{\mathrm{d}i_a^{(V2)}}{\mathrm{d}t} - e_a^{(V2)} \quad (70)$$

Finally, when $V3$ is applied as shown in Fig. 7c, the following equations hold true:

$$0 = r_s * i_a^{(V3)} + l_{\sigma a} * \frac{\mathrm{d}i_a^{(V3)}}{\mathrm{d}t} + e_a^{(V3)} - r_s * i_b^{(V3)} - l_{\sigma b} * \frac{\mathrm{d}i_b^{(V3)}}{\mathrm{d}t} - e_b^{(V3)} \quad (71)$$

$$\mathrm{V}_{DC} = r_s * i_b^{(V3)} + l_{\sigma b} * \frac{\mathrm{d}i_b^{(V4)}}{\mathrm{d}t} + e_b^{(V3)} - r_s * i_c^{(V3)} - l_{\sigma c} * \frac{\mathrm{d}i_c^{(V3)}}{\mathrm{d}t} - e_c^{(V3)} \quad (72)$$

$$0 = r_s * i_c^{(V3)} + l_{\sigma c} * \frac{\mathrm{d}i_c^{(V3)}}{\mathrm{d}t} + e_c^{(V3)} - r_s * i_d^{(V3)} - l_{\sigma d} * \frac{\mathrm{d}i_d^{(V3)}}{\mathrm{d}t} - e_d^{(V3)} \quad (73)$$

$$-\mathrm{V}_{DC} = r_s * i_d^{(V3)} + l_{\sigma d} * \frac{\mathrm{d}i_d^{(V3)}}{\mathrm{d}t} + e_d^{(V3)} - r_s * i_e^{(V3)} - l_{\sigma e} * \frac{\mathrm{d}i_e^{(V3)}}{\mathrm{d}t} - e_e^{(V3)} \quad (74)$$

$$0 = r_s * i_e^{(V3)} + l_{\sigma e} * \frac{\mathrm{d}i_e^{(V3)}}{\mathrm{d}t} + e_e^{(V3)} - r_s * i_a^{(V3)} - l_{\sigma a} * \frac{\mathrm{d}i_a^{(V3)}}{\mathrm{d}t} - e_a^{(V3)} \quad (75)$$

Table 1 Selection of P_a, P_b, P_c, P_d, and P_e for a star-connected five machine by sampling switching actions of active vector $V1$ and $V4$

Sector no	P_a	P_b	P_c	P_d	P_e
1	$\frac{\mathrm{d}i_c^{(V0)}}{\mathrm{d}t} - \frac{\mathrm{d}i_c^{(V4)}}{\mathrm{d}t}$	$\frac{\mathrm{d}i_e^{(V0)}}{\mathrm{d}t} - \frac{\mathrm{d}i_e^{(V4)}}{\mathrm{d}t}$	$\frac{\mathrm{d}i_e^{(V1)}}{\mathrm{d}t} - \frac{\mathrm{d}i_e^{(V0)}}{\mathrm{d}t}$	$\frac{\mathrm{d}i_b^{(V1)}}{\mathrm{d}t} - \frac{\mathrm{d}i_b^{(V0)}}{\mathrm{d}t}$	$-(P_a + P_b + P_c + P_d)$
2	$\frac{\mathrm{d}i_c^{(V0)}}{\mathrm{d}t} - \frac{\mathrm{d}i_c^{(V4)}}{\mathrm{d}t}$	$\frac{\mathrm{d}i_e^{(V0)}}{\mathrm{d}t} - \frac{\mathrm{d}i_e^{(V4)}}{\mathrm{d}t}$	$-(P_a + P_b + P_d + P_e)$	$\frac{\mathrm{d}i_a^{(V1)}}{\mathrm{d}t} - \frac{\mathrm{d}i_a^{(V0)}}{\mathrm{d}t}$	$\frac{\mathrm{d}i_c^{(V1)}}{\mathrm{d}t} - \frac{\mathrm{d}i_{ac}^{(V0)}}{\mathrm{d}t}$
3	$-(P_b + P_c + P_d + P_e)$	$\frac{\mathrm{d}i_d^{(V0)}}{\mathrm{d}t} - \frac{\mathrm{d}i_d^{(V4)}}{\mathrm{d}t}$	$\frac{\mathrm{d}i_a^{(V0)}}{\mathrm{d}t} - \frac{\mathrm{d}i_a^{(V4)}}{\mathrm{d}t}$	$\frac{\mathrm{d}i_a^{(V1)}}{\mathrm{d}t} - \frac{\mathrm{d}i_a^{(V0)}}{\mathrm{d}t}$	$\frac{\mathrm{d}i_c^{(V1)}}{\mathrm{d}t} - \frac{\mathrm{d}i_c^{(V0)}}{\mathrm{d}t}$
4	$\frac{\mathrm{d}i_d^{(V1)}}{\mathrm{d}t} - \frac{\mathrm{d}i_d^{(V0)}}{\mathrm{d}t}$	$\frac{\mathrm{d}i_d^{(V0)}}{\mathrm{d}t} - \frac{\mathrm{d}i_d^{(V4)}}{\mathrm{d}t}$	$\frac{\mathrm{d}i_a^{(V0)}}{\mathrm{d}t} - \frac{\mathrm{d}i_a^{(V4)}}{\mathrm{d}t}$	$-(P_a + P_b + P_c + P_e)$	$\frac{\mathrm{d}i_b^{(V1)}}{\mathrm{d}t} - \frac{\mathrm{d}i_{ab}^{(V0)}}{\mathrm{d}t}$
5	$\frac{\mathrm{d}i_d^{(V1)}}{\mathrm{d}t} - \frac{\mathrm{d}i_d^{(V0)}}{\mathrm{d}t}$	$-(P_a + P_c + P_d + P_e)$	$\frac{\mathrm{d}i_e^{(V0)}}{\mathrm{d}t} - \frac{\mathrm{d}i_e^{(V4)}}{\mathrm{d}t}$	$\frac{\mathrm{d}i_b^{(V0)}}{\mathrm{d}t} - \frac{\mathrm{d}i_b^{(V4)}}{\mathrm{d}t}$	$\frac{\mathrm{d}i_b^{(V1)}}{\mathrm{d}t} - \frac{\mathrm{d}i_{ab}^{(V0)}}{\mathrm{d}t}$
6	$\frac{\mathrm{d}i_c^{(V1)}}{\mathrm{d}t} - \frac{\mathrm{d}i_c^{(V0)}}{\mathrm{d}t}$	$\frac{\mathrm{d}i_e^{(V1)}}{\mathrm{d}t} - \frac{\mathrm{d}i_e^{(V0)}}{\mathrm{d}t}$	$\frac{\mathrm{d}i_e^{(V0)}}{\mathrm{d}t} - \frac{\mathrm{d}i_e^{(V4)}}{\mathrm{d}t}$	$\frac{\mathrm{d}i_b^{(V0)}}{\mathrm{d}t} - \frac{\mathrm{d}i_b^{(V4)}}{\mathrm{d}t}$	$-(P_a + P_b + P_c + P_d)$
7	$\frac{\mathrm{d}i_c^{(V1)}}{\mathrm{d}t} - \frac{\mathrm{d}i_c^{(V0)}}{\mathrm{d}t}$	$\frac{\mathrm{d}i_e^{(V1)}}{\mathrm{d}t} - \frac{\mathrm{d}i_e^{(V0)}}{\mathrm{d}t}$	$-(P_a + P_b + P_d + P_e)$	$\frac{\mathrm{d}i_a^{(V0)}}{\mathrm{d}t} - \frac{\mathrm{d}i_a^{(V4)}}{\mathrm{d}t}$	$\frac{\mathrm{d}i_c^{(V0)}}{\mathrm{d}t} - \frac{\mathrm{d}i_c^{(V4)}}{\mathrm{d}t}$
8	$-(P_b + P_c + P_d + P_e)$	$\frac{\mathrm{d}i_d^{(V1)}}{\mathrm{d}t} - \frac{\mathrm{d}i_d^{(V0)}}{\mathrm{d}t}$	$\frac{\mathrm{d}i_a^{(V1)}}{\mathrm{d}t} - \frac{\mathrm{d}i_a^{(V0)}}{\mathrm{d}t}$	$\frac{\mathrm{d}i_a^{(V0)}}{\mathrm{d}t} - \frac{\mathrm{d}i_a^{(V4)}}{\mathrm{d}t}$	$\frac{\mathrm{d}i_c^{(V0)}}{\mathrm{d}t} - \frac{\mathrm{d}i_c^{(V4)}}{\mathrm{d}t}$
9	$\frac{\mathrm{d}i_d^{(V0)}}{\mathrm{d}t} - \frac{\mathrm{d}i_d^{(V4)}}{\mathrm{d}t}$	$\frac{\mathrm{d}i_d^{(V1)}}{\mathrm{d}t} - \frac{\mathrm{d}i_d^{(V0)}}{\mathrm{d}t}$	$\frac{\mathrm{d}i_a^{(V1)}}{\mathrm{d}t} - \frac{\mathrm{d}i_a^{(V0)}}{\mathrm{d}t}$	$-(P_a + P_b + P_c + P_e)$	$\frac{\mathrm{d}i_b^{(V0)}}{\mathrm{d}t} - \frac{\mathrm{d}i_b^{(V4)}}{\mathrm{d}t}$
10	$\frac{\mathrm{d}i_d^{(V0)}}{\mathrm{d}t} - \frac{\mathrm{d}i_d^{(V4)}}{\mathrm{d}t}$	$-(P_a + P_c + P_d + P_e)$	$\frac{\mathrm{d}i_e^{(V1)}}{\mathrm{d}t} - \frac{\mathrm{d}i_e^{(V0)}}{\mathrm{d}t}$	$\frac{\mathrm{d}i_b^{(V1)}}{\mathrm{d}t} - \frac{\mathrm{d}i_b^{(V0)}}{\mathrm{d}t}$	$\frac{\mathrm{d}i_b^{(V0)}}{\mathrm{d}t} - \frac{\mathrm{d}i_b^{(V4)}}{\mathrm{d}t}$

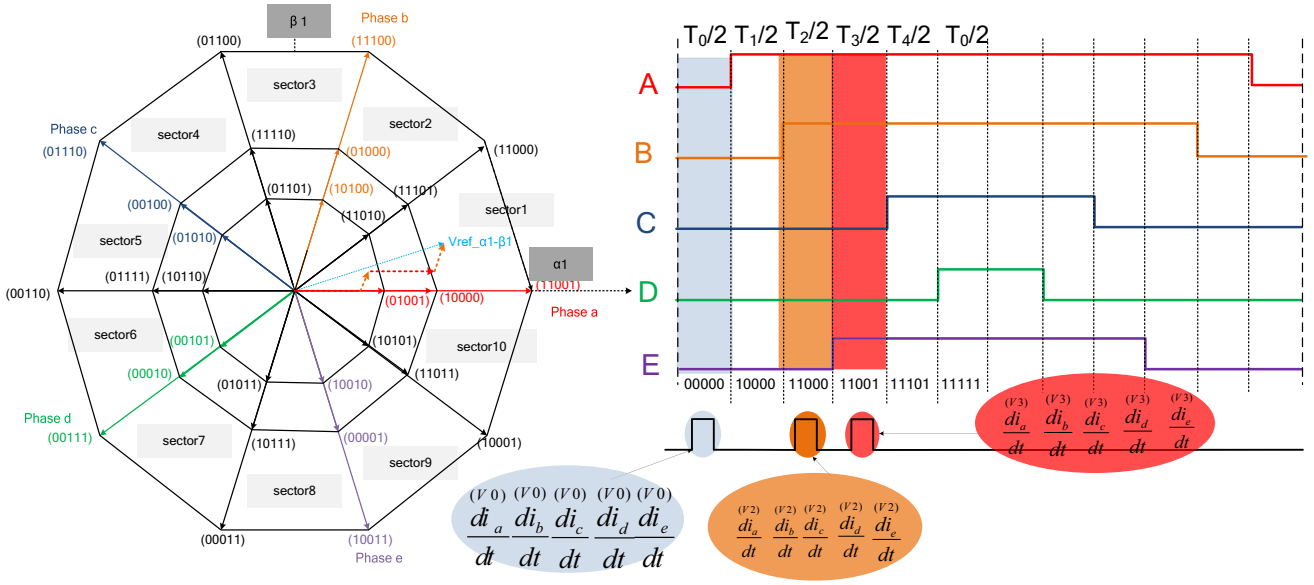

Fig. 6 Sampling time of the currents responses due to the switching actions of active vector $V2$ and $V3$ in case that V_ref_α1-β1 exists in first sector

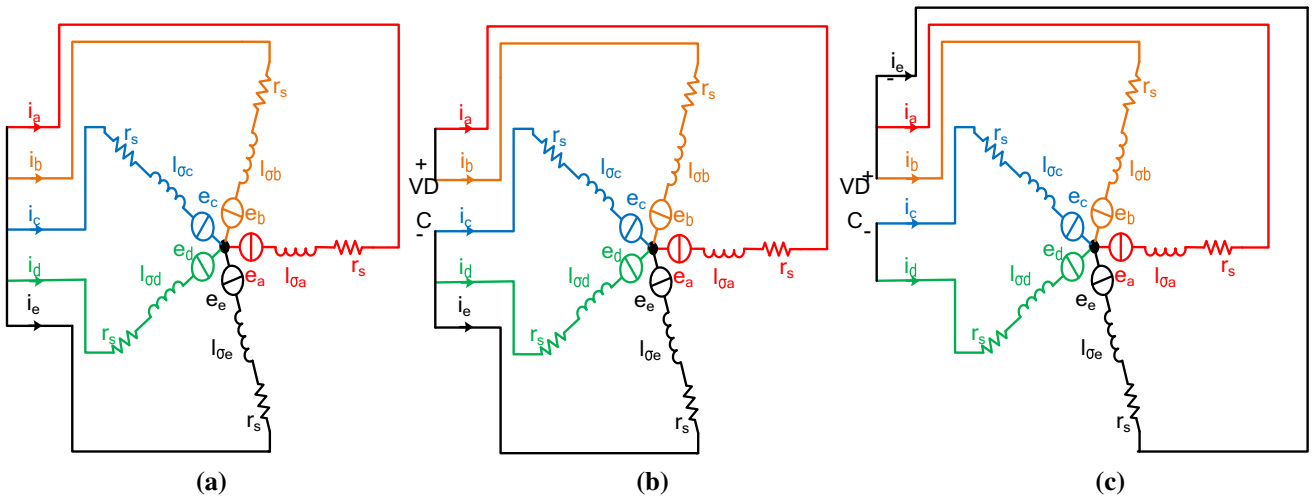

Fig. 7 Stator circuits when: **a** $V0$ is applied; **b** $V2$ is applied; **c** $V3$ is applied

Assuming that the voltage drop across the stator resistances is small and the back emf can be neglected providing the time separation between the vectors is small, the following equations can be obtained using vector $V2$, $V3$, and $V0$:

$$P_a = -\left(\frac{\mathrm{d}i_c^{(V2)}}{\mathrm{d}t} - \frac{\mathrm{d}i_c^{(V0)}}{\mathrm{d}t}\right) = 2 * C1 + 1.45 * C2 * \cos(2\theta) \quad (76)$$

$$P_b = -\left(\frac{\mathrm{d}i_e^{(V2)}}{\mathrm{d}t} - \frac{\mathrm{d}i_e^{(V0)}}{\mathrm{d}t}\right) = 2 * C1 + 1.45 * C2 * \cos\left(2\theta - 72^\circ\right) \quad (77)$$

$$P_c = \left(\frac{\mathrm{d}i_e^{(V3)}}{\mathrm{d}t} - \frac{\mathrm{d}i_e^{(V0)}}{\mathrm{d}t}\right) = 2 * C1 + 1.45 * C2 * \cos\left(2\theta - 144^\circ\right) \quad (78)$$

$$P_d = \left(\frac{\mathrm{d}i_b^{(V3)}}{\mathrm{d}t} - \frac{\mathrm{d}i_b^{(V0)}}{\mathrm{d}t}\right) = 2 * C1 + 1.45 * C2 * \cos\left(2\theta - 216^\circ\right) \quad (79)$$

The estimated position signal P_a, P_b, P_c, P_d, and P_e in other sectors can be obtained using the same technique as shown in Table 2.

The position scalars P_a, P_b, P_c, P_d, and P_e either obtained from Tables 1 or 2 can be transformed into P_α, P_β and can

Table 2 Selection of P_a, P_b, P_c, P_d, and P_e for a star-connected five machine by sampling switching actions of active vector $V2$ and $V3$

Sector no	P_a	P_b	P_c	P_d	P_e
1	$\frac{\mathrm{d}i_c^{(V0)}}{\mathrm{d}t} - \frac{\mathrm{d}i_c^{(V2)}}{\mathrm{d}t}$	$\frac{\mathrm{d}i_e^{(V0)}}{\mathrm{d}t} - \frac{\mathrm{d}i_e^{(V2)}}{\mathrm{d}t}$	$\frac{\mathrm{d}i_e^{(V3)}}{\mathrm{d}t} - \frac{\mathrm{d}i_e^{(V0)}}{\mathrm{d}t}$	$\frac{\mathrm{d}i_b^{(V3)}}{\mathrm{d}t} - \frac{\mathrm{d}i_b^{(V0)}}{\mathrm{d}t}$	$-(P_a + P_b + P_c + P_d)$
2	$\frac{\mathrm{d}i_c^{(V0)}}{\mathrm{d}t} - \frac{\mathrm{d}i_c^{(V2)}}{\mathrm{d}t}$	$\frac{\mathrm{d}i_e^{(V0)}}{\mathrm{d}t} - \frac{\mathrm{d}i_e^{(V2)}}{\mathrm{d}t}$	$-(P_a + P_b + P_d + P_e)$	$\frac{\mathrm{d}i_a^{(V3)}}{\mathrm{d}t} - \frac{\mathrm{d}i_a^{(V0)}}{\mathrm{d}t}$	$\frac{\mathrm{d}i_c^{(V3)}}{\mathrm{d}t} - \frac{\mathrm{d}i_{ac}^{(V0)}}{\mathrm{d}t}$
3	$-(P_b + P_c + P_d + P_e)$	$\frac{\mathrm{d}i_d^{(V0)}}{\mathrm{d}t} - \frac{\mathrm{d}i_d^{(V2)}}{\mathrm{d}t}$	$\frac{\mathrm{d}i_a^{(V0)}}{\mathrm{d}t} - \frac{\mathrm{d}i_a^{(2)}}{\mathrm{d}t}$	$\frac{\mathrm{d}i_a^{(V3)}}{\mathrm{d}t} - \frac{\mathrm{d}i_a^{(V0)}}{\mathrm{d}t}$	$\frac{\mathrm{d}i_c^{(V3)}}{\mathrm{d}t} - \frac{\mathrm{d}i_c^{(V0)}}{\mathrm{d}t}$
4	$\frac{\mathrm{d}i_d^{(V3)}}{\mathrm{d}t} - \frac{\mathrm{d}i_d^{(V0)}}{\mathrm{d}t}$	$\frac{\mathrm{d}i_d^{(V0)}}{\mathrm{d}t} - \frac{\mathrm{d}i_d^{(V2)}}{\mathrm{d}t}$	$\frac{\mathrm{d}i_a^{(V0)}}{\mathrm{d}t} - \frac{\mathrm{d}i_a^{(V2)}}{\mathrm{d}t}$	$-(P_a + P_b + P_c + P_e)$	$\frac{\mathrm{d}i_b^{(V3)}}{\mathrm{d}t} - \frac{\mathrm{d}i_{ab}^{(V0)}}{\mathrm{d}t}$
5	$\frac{\mathrm{d}i_d^{(V3)}}{\mathrm{d}t} - \frac{\mathrm{d}i_d^{(V0)}}{\mathrm{d}t}$	$-(P_a + P_c + P_d + P_e)$	$\frac{\mathrm{d}i_e^{(V0)}}{\mathrm{d}t} - \frac{\mathrm{d}i_e^{(V2)}}{\mathrm{d}t}$	$\frac{\mathrm{d}i_b^{(V0)}}{\mathrm{d}t} - \frac{\mathrm{d}i_b^{(V2)}}{\mathrm{d}t}$	$\frac{\mathrm{d}i_b^{(V3)}}{\mathrm{d}t} - \frac{\mathrm{d}i_{ab}^{(V0)}}{\mathrm{d}t}$
6	$\frac{\mathrm{d}i_c^{(V3)}}{\mathrm{d}t} - \frac{\mathrm{d}i_c^{(V0)}}{\mathrm{d}t}$	$\frac{\mathrm{d}i_e^{(V3)}}{\mathrm{d}t} - \frac{\mathrm{d}i_e^{(V0)}}{\mathrm{d}t}$	$\frac{\mathrm{d}i_e^{(V0)}}{\mathrm{d}t} - \frac{\mathrm{d}i_e^{(V2)}}{\mathrm{d}t}$	$\frac{\mathrm{d}i_b^{(V0)}}{\mathrm{d}t} - \frac{\mathrm{d}i_b^{(V2)}}{\mathrm{d}t}$	$-(P_a + P_b + P_c + P_d)$
7	$\frac{\mathrm{d}i_c^{(V3)}}{\mathrm{d}t} - \frac{\mathrm{d}i_c^{(V0)}}{\mathrm{d}t}$	$\frac{\mathrm{d}i_e^{(V3)}}{\mathrm{d}t} - \frac{\mathrm{d}i_e^{(V0)}}{\mathrm{d}t}$	$-(P_a + P_b + P_d + P_e)$	$\frac{\mathrm{d}i_a^{(V0)}}{\mathrm{d}t} - \frac{\mathrm{d}i_a^{(V2)}}{\mathrm{d}t}$	$\frac{\mathrm{d}i_c^{(V0)}}{\mathrm{d}t} - \frac{\mathrm{d}i_c^{(V2)}}{\mathrm{d}t}$
8	$-(P_b + P_c + P_d + P_e)$	$\frac{\mathrm{d}i_d^{(V3)}}{\mathrm{d}t} - \frac{\mathrm{d}i_d^{(V0)}}{\mathrm{d}t}$	$\frac{\mathrm{d}i_a^{(V3)}}{\mathrm{d}t} - \frac{\mathrm{d}i_a^{(V0)}}{\mathrm{d}t}$	$\frac{\mathrm{d}i_a^{(V0)}}{\mathrm{d}t} - \frac{\mathrm{d}i_a^{(V2)}}{\mathrm{d}t}$	$\frac{\mathrm{d}i_c^{(V0)}}{\mathrm{d}t} - \frac{\mathrm{d}i_c^{(V2)}}{\mathrm{d}t}$
9	$\frac{\mathrm{d}i_d^{(V0)}}{\mathrm{d}t} - \frac{\mathrm{d}i_d^{(V2)}}{\mathrm{d}t}$	$\frac{\mathrm{d}i_d^{(V3)}}{\mathrm{d}t} - \frac{\mathrm{d}i_d^{(V0)}}{\mathrm{d}t}$	$\frac{\mathrm{d}i_a^{(V3)}}{\mathrm{d}t} - \frac{\mathrm{d}i_a^{(V0)}}{\mathrm{d}t}$	$-(P_a + P_b + P_c + P_e)$	$\frac{\mathrm{d}i_b^{(V0)}}{\mathrm{d}t} - \frac{\mathrm{d}i_b^{(V2)}}{\mathrm{d}t}$
10	$\frac{\mathrm{d}i_d^{(V0)}}{\mathrm{d}t} - \frac{\mathrm{d}i_d^{(V2)}}{\mathrm{d}t}$	$-(P_a + P_c + P_d + P_e)$	$\frac{\mathrm{d}i_e^{(V3)}}{\mathrm{d}t} - \frac{\mathrm{d}i_e^{(V0)}}{\mathrm{d}t}$	$\frac{\mathrm{d}i_b^{(V3)}}{\mathrm{d}t} - \frac{\mathrm{d}i_b^{(V0)}}{\mathrm{d}t}$	$\frac{\mathrm{d}i_b^{(V0)}}{\mathrm{d}t} - \frac{\mathrm{d}i_b^{(V2)}}{\mathrm{d}t}$

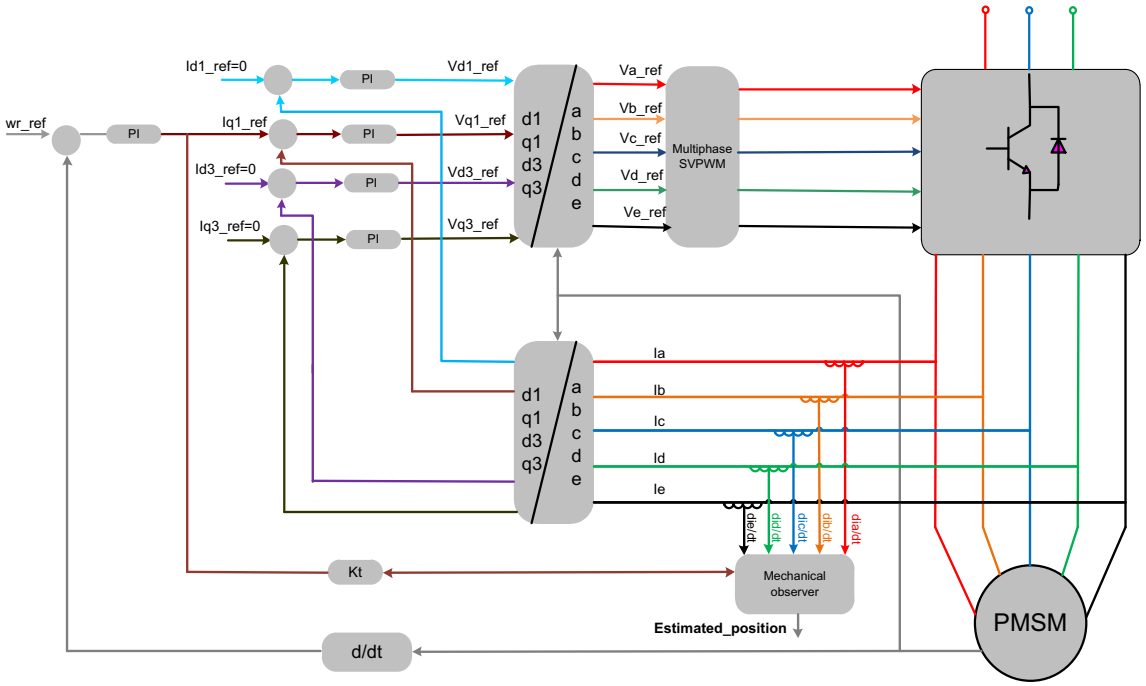

Fig. 8 Saliency tracking control topology for five-phase drive

then be used to denote the orientation angle as follows :

$$\begin{bmatrix} P_\alpha \\ P_\beta \end{bmatrix} = [V] \begin{bmatrix} a \\ b \\ c \\ d \\ e \end{bmatrix} \left(\frac{\mathrm{d}i_d^{(V4)}}{\mathrm{d}t} - \frac{\mathrm{d}i_d^{(V0)}}{\mathrm{d}t} \right), \tag{80}$$

where

$$V = \begin{bmatrix} 1 & \cos\left(216^\circ\right) & \cos\left(72^\circ\right) & \cos\left(288^\circ\right) & \cos\left(144^\circ\right) \\ 0 & \sin\left(216^\circ\right) & \sin\left(72^\circ\right) & \sin(288) & \sin\left(144^\circ\right) \end{bmatrix} \tag{81}$$

3 Results and analysis

3.1 Position and speed estimation under sensored operation

The validation of the saliency tracking algorithms given in Tables 1 and 2 is obtained using the vector control structure working in a sensored mode shown in Fig. 8. To make the design more practical, a mechanical observer [23] is used to filter out the high-frequency noise in the position signals. This noise is caused by differentiating the stator currents to obtain the di/dt signals. The whole vector control structure has been implemented in simulation in the Saber modeling environment. The simulation includes a minimum pulse width of 10 us when di/dt measurements are taken. This is a realistic values seen from experimental results of [22].

The results shown in Fig. 9 demonstrate the validity of the saliency tracking algorithms. The motor was running at 120 rpm speed and at half load. At $t = 2$ s, a speed step change from 120 to 0 rpm was applied to the system. Then at $t = 3$ s, another speed step change from 0 to -120 rpm was introduced to the system. At $t = 5$ s, a zero speed was applied to the system and finally at $t = 6$ s, a speed step change from 0 to 120 rpm was applied to the system. The algorithm that is used to track the saliency from $t = 1$–4 s is the one given in Table 1 (using $V1$, $V4$ and $V0$), while the algorithm that is given in Table 2 (using $V2$, $V3$ and $V0$) is used to track the saliency for the rest of the test. The results show that the motor responded to the load and speed steps very fast and the proposed algorithms could track the saturation saliency (2*fe) at positive, negative, and more importantly at low and zero speeds. Finally, the position scalars P_a, P_b, P_c, P_d, and P_e obtained from the algorithm given in Table 2 have higher amplitude compared to those obtained from the algorithm given in Table 1, and hence it can be said that first advantage of using the algorithm, given in Table 2 over using the algorithm given in Table 1, is the higher signal-to-noise ratio.

Fully Sensorless Speed Control

The speed control for a five-phase PM machine drive has been implemented in simulation in the Saber modeling environment. This estimated speed $\omega_r^{\wedge}$ and position $\theta_r^{\wedge}$ are used to obtain a fully sensorless speed control as shown in Fig. 10.

Figure 11 shows the results of a fully sensorless speed control of a five-phase PMSM motor driven by a five-phase

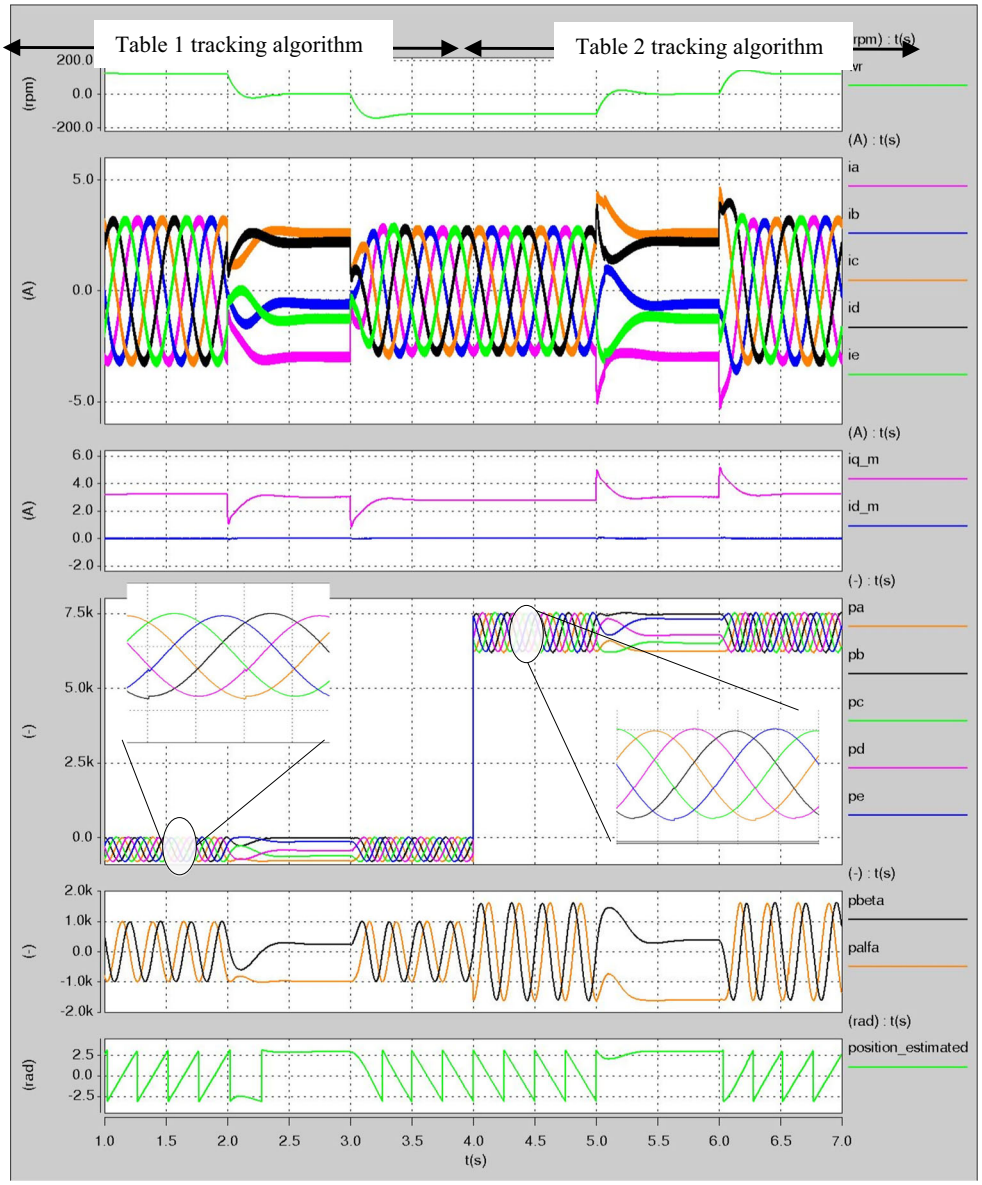

Fig. 9 Saliency tracking results

inverter at a half load condition using the algorithms presented in this paper. The motor was working in sensorless mode at speed = 1 Hz, then at $t = 6$ s, a speed step change from 1 Hz to 0 rpm (till $t = 8$ s) is applied to the system. The algorithm that is given in Table 1 is used to track the saliency from the begging till $t = 7$ s. Then the algorithm that is given in Table 2 is used for the rest of the test. Figure 11 shows that the motor responded to the speed step with a good transient and steady-state response regardless which algorithm is used to track the saliency.

Figure 12 demonstrates the stability of the fully sensorless system when a load disturbance was applied. The motor was running at zero speed and at no load in sensorless mode. Then a step change from 0 to 100 rpm is applied to the system at $t = 2$ s. A full load step is applied to the motor at $t = 3$ s. At $t = 5$ s, a speed step change from 100 to 0 rpm is applied to the system. At $t = 5$ s, the motor became unloaded. At $t = 7$ s, a full load step is applied again to the system. At $t = 8$ s, a speed step change from 0 to 100 rpm is applied to the system. After that at $t = 9$ s, the motor became unloaded again. Finally, at $t = 10$ s, a speed step change from 100 rpm to zero is applied to the system. The algorithm given in Table 1 is used to track the saliency from the begging till $t = 7$ s; then, the algorithm given in Table 2 is used for the rest of the test. The results show that the system maintained the speed in all the cases.

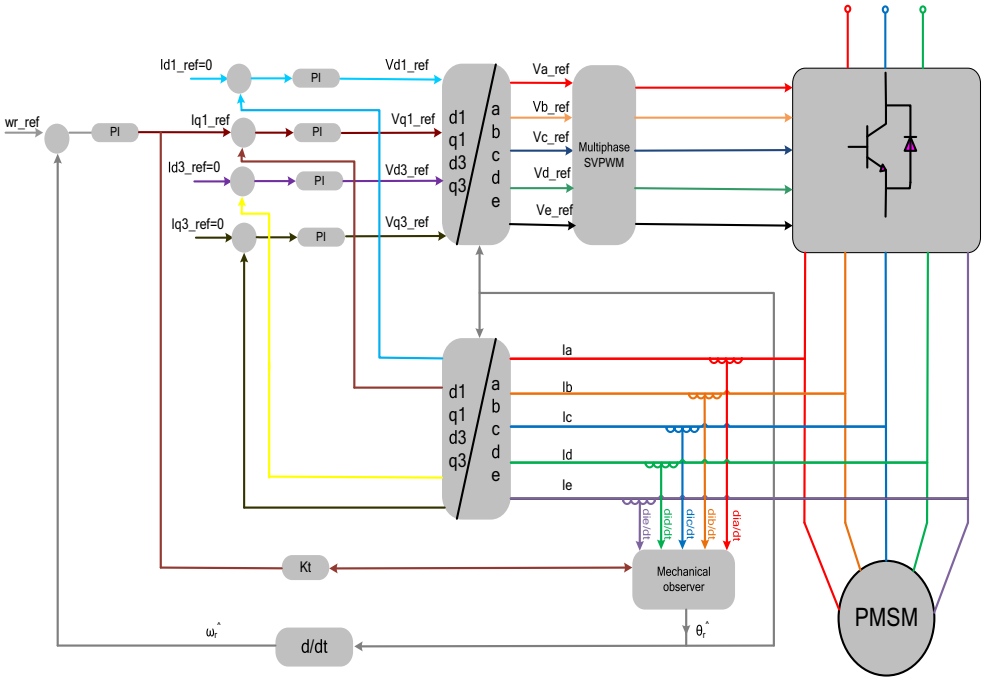

Fig. 10 Sensorless vector control structure for the five-phase inverter PMSM drive

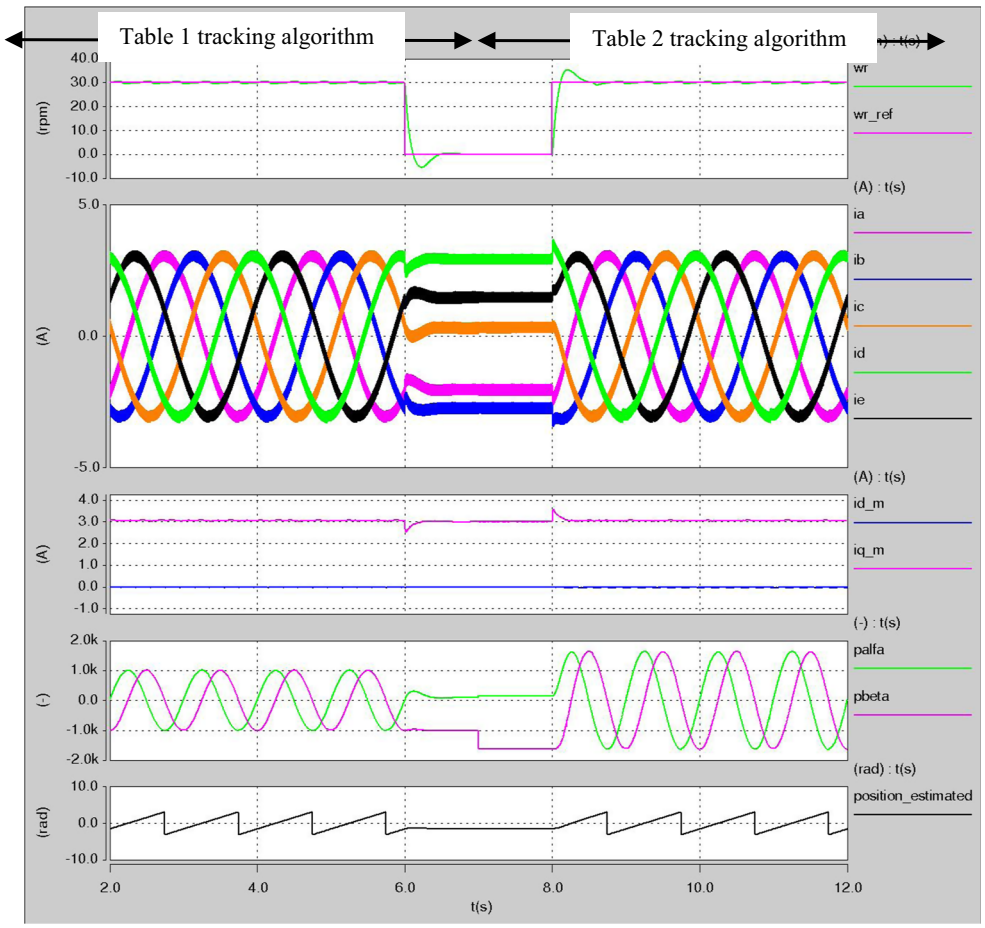

Fig. 11 Fully sensorless speed steps between 0.5, 0, and 0.5 Hz at half load

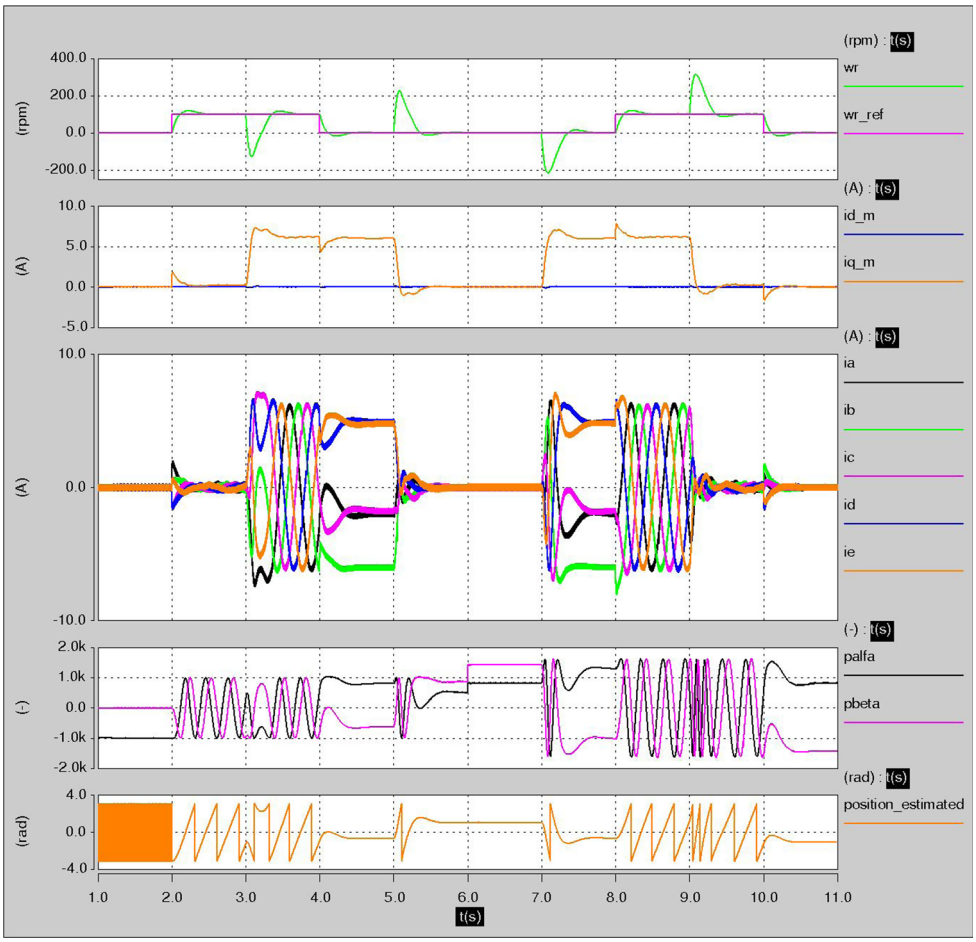

Fig. 12 Fully sensorless full load steps

3.2 Current distortion reduction

The main difficulty when applying current derivative-based position estimation schemes to real systems arises from the parasitic effects within the motor, the inverter, and the cabling [24]. And hence, narrow active voltage vectors must be extended to a minimum vector duration t_{min} which is set according to the high-frequency decay. In this paper, t_{min} is set to 10 us. This means that the active vector $V1$ and $V4$ in case of using the algorithm given in Table 1 (Fig. 13a) should be extended to t_{min} if the time duration is less than t_{min}. Also, the active vectors $V2$ and $V3$ in case of using the algorithm given in Table 2 (Fig 13b) should be extended to t_{min} if the time duration of any of them is less than that t_{min}.

The time duration ($T0$, $T1$, $T2$, $T3$, and $T4$) of the active vectors shown in Fig 13b is obtained using Eqs (37–39). It should be highlighted that when the phase voltage is sinusoidal, or the magnitude of the $d3q3$-axes voltage vector is zero as in our case, the following equations hold true [12]:

$$T3 = 1.618 * T1 \tag{82}$$

$$T2 = 1.618 * T4 \tag{83}$$

This means that the extension of the vectors $V2$ and $V3$ will be less than that of the vectors $V1$ and $V4$ which help to reduce the current distortion introduced to the motor stator currents as shown in Fig. 14a–c. Figure 14a demonstrates the sequence of applying the active vectors $V1$, $V2$, $V3$, $V4$ to generate the reference voltage $V_{ref}\_\alpha 1 - -\beta 1$ if it exists in the first sector in the normal case (without extensions). In Fig. 14b, the active vectors $V1$ and $V4$ are extended to t_{min}, and finally, in Fig. 14c, the active $V2$ and $V3$ are extended to t_{min}. From the figure, it is quite clear that the voltage ripples (gray areas) in the case of extending the active vectors $V2$ and $V3$ is less than those in the case of extending the active vectors $V1$ and $V4$ and therefore less current distortion will be introduced to the motor stator currents.

The above idea is demonstrated using Saber simulator as shown in Fig. 15. The motor was running at 400 rpm without any extensions to any of the active vectors. From $t = 1.8$ to 2.1 s active vectors $V1$ and $V4$ are extended according to the algorithm that is given in Table 1. Finally, from $t = 2.1$ s to the end, active vectors $V2$ and $V3$ are extended according to the algorithm that is given in Table 2. It is clear from the waveform of the stator current ib that the extension of the active vectors $V2$ and $V3$ between $t = 2.1$ s till 2.4 s

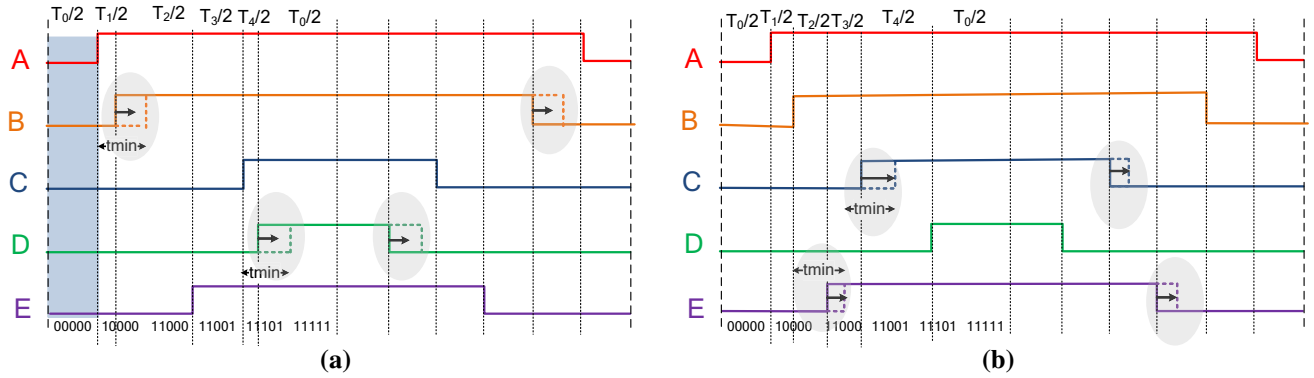

Fig. 13 Space vector modulation state diagram for five-phase inverter in case that V_ref_α1-β1 exists in first sector **a** $V1$ and $V4$ are extended as in Table 1, **b** $V2$, and $V3$ are extended as in Table 2

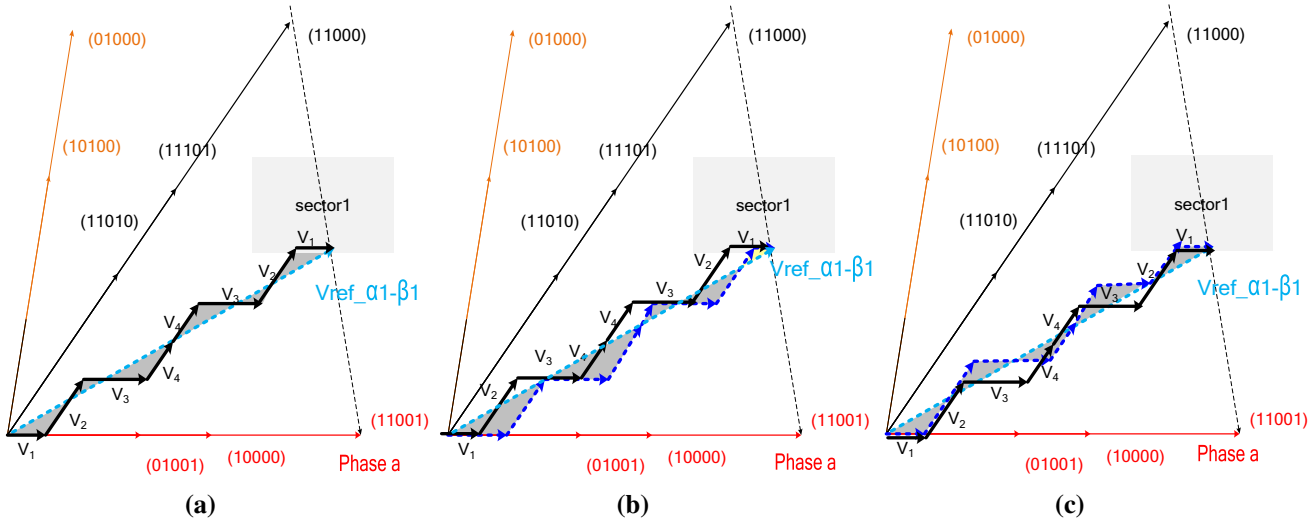

Fig. 14 Current ripple for different extension schemes. **a** No extensions. **b** Extension of active vectors $V1$ and $V4$. **c** Extension of active vectors $V2$ and $V3$

is introducing less distortion to the stator current compared to the extension of the active vectors $V1$ and $V4$ between $t = 1.8$ s and $t = 2.1$ s. This due to the fact that between $t = 2.1$ s and $t = 2.4$ s, 10% of the PWM periods have at least active vectors ($V2$ or $V3$) longer than t_{min}, while all PWM periods between $t = 1.8$ and $t = 2$ s need to extend both vectors $V1$ and $V4$. Moreover, the length of the vector $V2$ and $V3$ as shown in Fig. 15 is greater than the length of the active vectors $V1$ and $V4$ which makes the extension of the vectors $V2$ and $V3$ less.

The FFT of the current waveforms in Fig. 15 is given Fig. 16a–c . The results prove the advantage of the extension of $V2$ and $V3$ over the extension of active vectors $V1$ and $V4$ in terms of current distortion.

4 Conclusion

This paper has outlined two new algorithms for tracking the saliency of motor fed by a five-leg inverter. The saliency is tracked through measuring the dynamic current response of the motor line currents due to the IGBT switching actions. The proposed methods include software modification to the method proposed in[18] to track the saliency of the motor fed by three-phase inverter . The two new algorithms can be used to track the saturation saliency in PM and the rotor slotting saliency in induction motors. The results have shown the advantages of using the switching action of the active vectors $V2$ and $V3$ over using the active vectors $V1$ and $V4$,

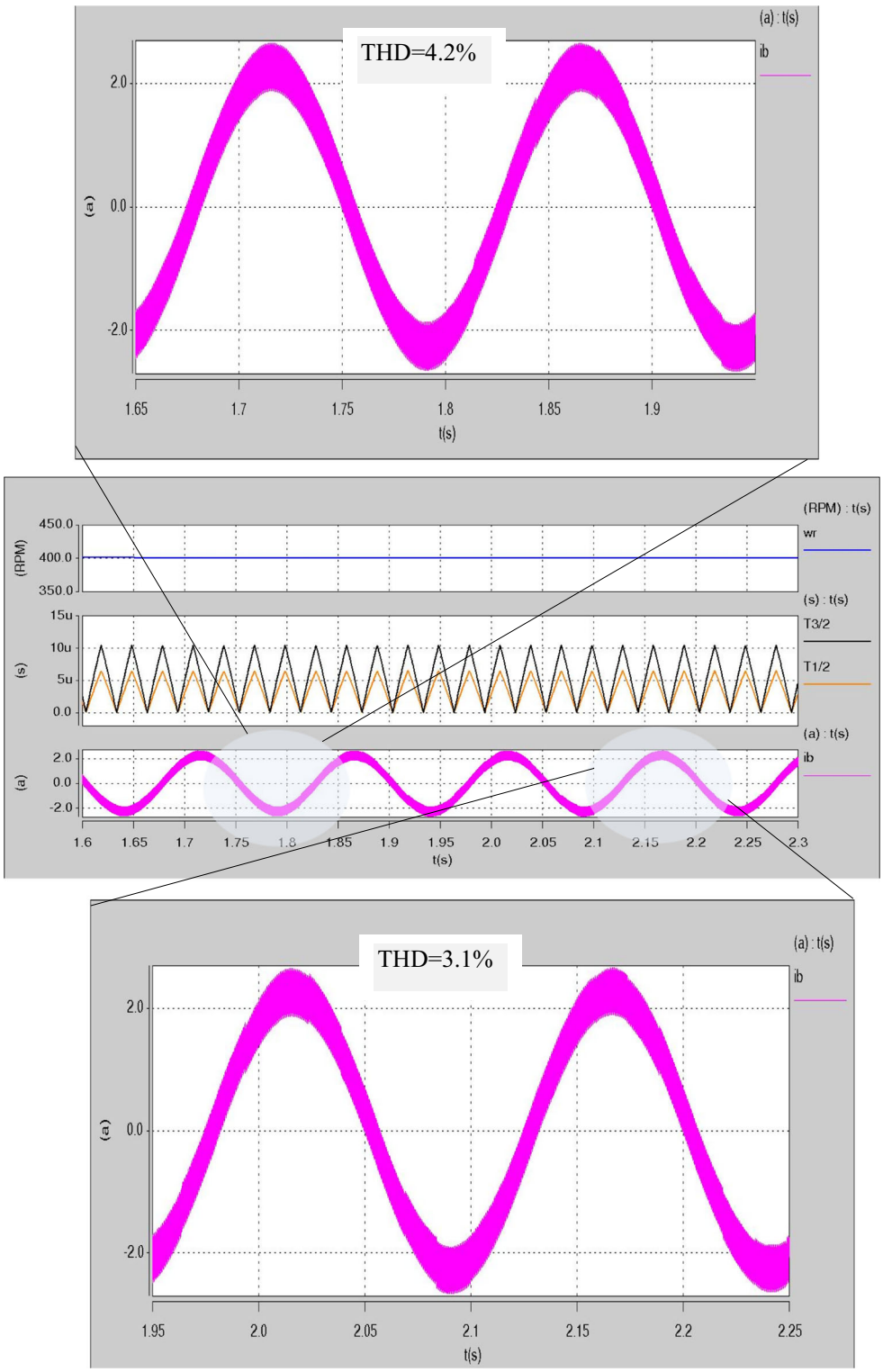

Fig. 15 Current waveform under different extension schemes

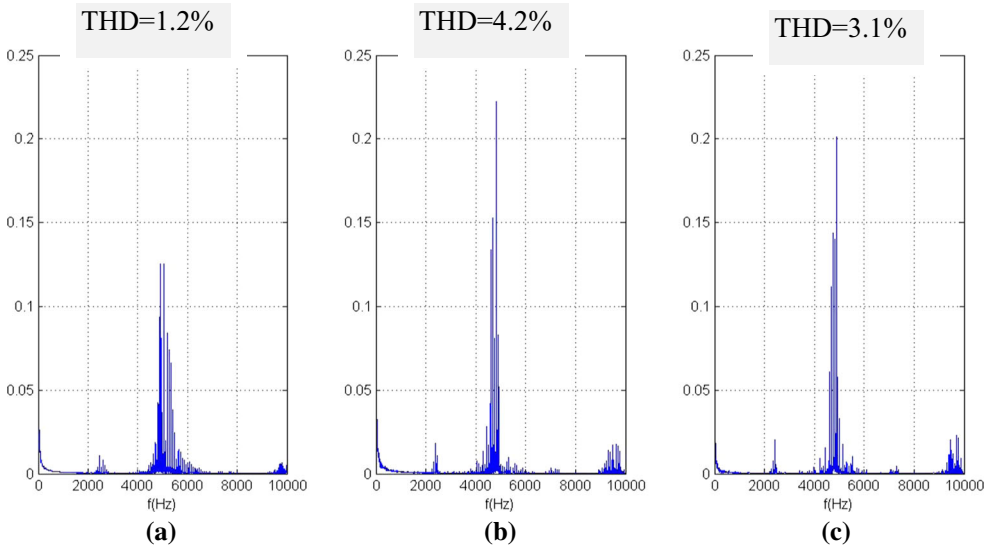

Fig. 16 FFT of the current waveform under different extension schemes. **a** No extensions. **b** Extension of active vectors $V1$ and $V4$. **c** Extension of vectors $V2$ and $V3$

in terms of the quality of the estimated position signals and the distortion introduced to the stator currents by extending the narrow vectors.

References

1. Villani M, Tursini M, Fabri G, Castellini L (2010) Multi-phase fault tolerant drives for aircraft applications. In: IEEE, electrical systems for aircraft, railway and ship propulsion conference (ESARS), Bologna, Italy. IEEE, New York, 19–21 Oct 2010
2. Qingguo S, Xiaofeng Z, Fei Y, Chengsheng Z (2005) Research on space vector PWM of five-phase three-level inverter. In: IEEE, electrical machines and systems conference (ICEMS), Nanjing, China. IEEE, New York, 29–29 Sep 2005
3. Ruhe S, Toliyat HA (2002) Vector control of five-phase synchronous reluctance motor with space vector pulse width modulation (SVPWM) for minimum switching losses. In: IEEE, applied power electronics conference and exposition (APEC) Dallas, Texas, USA. IEEE, New York, 10–14 March 2002
4. Abbas MA, Christen R, Jahns TM (1984) Six-phase voltage source inverter driven induction motor. IEEE Trans Ind Appl 20:1251–1259
5. Zhao X, Lipo TA (1995) Space vector PWM control of dual three-phase induction machine using vector space decomposition. IEEE Trans Ind Appl 31:1177–1184
6. Parsa L, Toliyat HA (2003) Multi-phase permanent magnet motor drives. In: IEEE, industry applications conference (IAS), Utah, USA. IEEE, New York, 12–16 Oct 2003
7. Xu H, Toliyat HA, Pertersen LJ (2002) Five-phase induction motor drives with DSP-based control system. IEEE Trans Ind Appl 17:524–533
8. Kelly JW, Strangas EG, Miller JM (2003) Multiphase space vector pulse width modulation. IEEE Trans Energy Convers 18:259–264
9. Xue S, Wen X, Feng Z (2006) A novel multi-dimensional SVPWM strategy of multiphase motor drives. In: EPE 2006 power electronics and motion control conference, Portoroz, Slovenia. Brigitte Sneyers, Pleinlaan 2, Brussels, Belgium: EPE, 30 Aug–1 Sep 2006
10. Pengfei W, Ping Z, Fan W, Jiawei Z, Tiecai L (2014) Research on dual-plane vector control of five phase fault-tolerant permanent magnet machine. In: IEEE, transportation electrification Asia-Pacific conference (ITEC Asia-Pacific), Beijing, China. IEEE, New York, 31 Aug–3 Sep 2014
11. Minghao T, Wei H, Ming CA (2014) Novel space vector modulation strategy for a five-phase flux-switching permanent magnet motor drive system. In: IEEE, electrical machines and systems conference (ICEMS), Hangzhou, China. IEEE, New York, 22–25 Oct 2014
12. Chen K-Y (2015) Multiphase pulse-width modulation considering reference order for sinusoidal wave production. In: IEEE, industrial electronics and applications conference (ICIEA) New Zealand, Auckland. IEEE, New York, 15–17 June 2015
13. El-Barbary ZMS (2012) DSP based vector control of five-phase induction motor using Fuzzy Logic Control. Int J Power Electron Drive Syst 2(2):192–202
14. Iqbal A, Moinoddin S, Rahman K (2015) Finite state predictive current and common mode voltage control of a seven-phase voltage source inverter. Int J Power Electron Drive Syst 6(3):459–476
15. Olivieri C, Fabri G, Tursini M (2010) Sensorless control of five-phase brushless DC motors. In: IEEE, sensorless control for electrical drives conference (SLED), Padova, Italy. IEEE, NewYork, 9–10 July 2010
16. Karampuri R, Prieto J, Barrero F, Jain S (2014) Extension of the DTC technique to multiphase induction motor drives using any odd number of phases. In: IEEE vehicle power and propulsion conference (VPPC), Coimbra, Portugal. IEEE, NewYork, 27–30 Oct 2014
17. Parsa L, Toliyat HA (2007) Sensorless direct torque control of five-phase interior permanent-magnet motor drives. IEEE Trans Ind Appl 43:952–959
18. wubin K, Jin H, Ming K, Bingnan L (2011) Research of sensorless control for multiphase induction motor based on high frequency injection signal technique. In: IEEE, electrical machines and systems conference (ICEMS), Beijing, China. IEEE, NewYork, 20–23 Aug 2011
19. Minglei G, Ogasawara S, Takemoto M (2013) An inductance estimation method for sensorless IPMSM drives based on multiphase SVPWM. In: IEEE, future energy electronics conference (IFEEC), Tainan, Taiwan. IEEE, NewYork, 3–6 Nov 2013

20. Schroedl M (1996) Sensorless control of AC machines at low speed and standstill based on the INFORM method. In: IEEE, industry applications conference, San Diego, USA. IEEE, New York, 6–10 Oct 1996
21. Holtz J, Juliet J (2004) Sensorless acquisition of the rotor position angle of induction motors with arbitrary stator winding. In: IEEE industry applications conference, Washington, USA. IEEE, NewYork, 3–7 Oct 2004
22. Qiang G, Asher GM, Sumner M, Makys P (2006) Position estimation of AC machines at all frequencies using only space vector PWM based excitation. In: IET International Conference on power electronics, machines and drives, Dublin, Ireland. Savoy Place, London, UK: IET, 4-6 April 2006
23. Lorenz RD, Van Patten KW (1991) High-resolution velocity estimation for all-digital, ac servo drives. IEEE Trans Ind Appl 27:701–705
24. Hua Y, Sumner M, Asher G, Gao Q, Saleh K (2011) Improved sensorless control of a permanent magnet machine using fundamental pulse width modulation excitation. IET Electr Power Appl 5(4):359–370